Mineral Petrol (2008) 93: 143–152
DOI 10.1007/s00710-007-0226-0
Printed in The Netherlands

Mineralogy and Petrology

Microstructure and photocatalytic activity of natural rutile from China for oxidation of methylene blue in water

X.-Y. Chuan[1], **A. H. Lu**[1], **J. Chen**[2], **N. Li**[1], **Y. J. Guo**[1]

[1] School of Earth and Space Science, Peking University, Beijing, P.R. China
[2] Electron Microscopy Laboratory, Peking University, Beijing, P.R. China

Received August 11 2007; Accepted November 19 2007; Published online April 14 2008

Editorial handling: A. Beran

Summary

Natural rutile from China was found to have good photocatalytic activity for methylene blue (MB). Under UV irradiation, 50% of MB was decomposed in three hours by natural rutile, 90% in 77 hours and 100% in 119 hours. The Brunauer-Emmett-Teller (BET) specific surface area of natural rutile was only $0.4495\,m^2/g$. In order to explain the decomposition of MB, rutile was characterized by XRD, FESEM and TEM, revealing a modulated structure. Crystal structural parameters are consistent with the data from JCPDS. Chemical composition approximates to $Ti_{1.019}O_2$. Photocatalytic properties of rutile are believed to relate to metal ionic substitution, vacancies and defects in its microstructure. Natural rutile is a practical photocatalyst, although its reaction rate is a fifth of anatase. Rutile might be effective and practical for a large-scale photocatalytic decomposition of organic pollutants in quiet and still waters (e.g. pools and lakes) since it is relatively cheap and widely available.

Introduction

Titanium oxides are very attractive materials for photocatalysis (Ohno et al., 2001). There are three polymorphs of TiO_2: rutile, anatase and brookite, of which rutile is by far the most common in nature, anatase less so and brookite rare (Jaffe, 1988; Chuan et al., 2004). Only anatase-type TiO_2 has attracted interest as a catalyst for

Correspondence: X.-Y. Chuan, School of Earth and Space Science, Peking University, Beijing 100871, P.R. China
e-mails: xychuan@pku.edu.cn, chuanxiuyun@hotmail.com

environmental remediation, since its photocatalytic activity shows promise for the decomposition of several organic pollutants, e.g. decomposition of acetaldehyde in air (Ollis and Al-Ekabi, 1993; Inagaki et al., 2001), decomposition of methylene blue and phenol in water (Tryba et al., 2003; Chuan et al., 2004), degradation of chlorinated organic compounds in water, feedstock etc. (Chachula and Liu, 2003).

However, anatase rarely occurs in nature and can only be produced at significant costs by industrial processes. Recently, rutile nanoparticles synthesized by thermal hydrolysis of $TiOCl_2$ (Li et al., 2004) and $TiCl_4$ aqueous solution (Sun et al., 2003), have been tried to decompose organic pollutants using photocatalysis. As the most common polymorphy of TiO_2 (Zack and Luvizotto, 2006), natural rutile has previously been considered as being inert as a photocatalyst and we know of no attempt to study its catalytic activity.

The implantation of metal atoms (e.g. Pt, V, Fe, Cu, Ag, Nb, Zn) into anatase improves its photocatalytic properties (Depero, 1993; Choi et al., 1994; Depero et al., 1994; Gao and Chambers, 1996; Sánchez et al., 1996; Jimmy and Rayund, 1997; Lin et al., 1999; Towle et al., 1999; Cristallo et al., 2001; Tsuji et al., 2002). However, no research on rutile with metal impurities related to the enhancement of photocatalytic activity has been done. The crystal structure of rutile is tetragonal, $P4_2/mnm$, $a_0 = 0.459$ nm, $c_0 = 0.296$ nm (JCPDS). As the most common polymorph of TiO_2 in nature, rutile could have numerous ionic substitutions of elements such as Nb^{5+}, Ta^{5+}, Fe^{2+}, Fe^{3+} in its crystal structure (Penn and Banfield, 1998, 1999; El Goresy et al., 2001). Rutile with substituted ionic sites (V^{5+} and Nb^{5+}; Li et al., 2003) may lead to a good photocatalytic material.

In the present paper, we examined the adsorption, microstructure and photocatalytic properties of natural rutile to decompose the organic molecule methylene blue. Natural materials represent a widely available and relatively cheap source.

Experimental

Natural rutile was selected from a rutile mine in a basalt in Shaanxi Province, China. It is a product that is sold commercially. The dark red–brown rutile powder was provided as grains 0.1–1.0 mm in size. The chemical composite of rutile was characterized by an Electron Probe Micro-Analyser (Joel JCXA-733 EPMA) using an acceleration voltage of 15 kV and a sample current of 20 nA, and calibrated using a rutile reference standard (Astimex Scientific Ltd., Toronto, Canada). The crystallinity of rutile was examined by X-ray diffraction (XRD) using CuKα radiation. The surface morphology and microstructure of the powders were observed by Field Emission Scanning Electron Microscopy (FESEM), Hitachi S-4700 at an accelerating voltage of 15 kV and a nominal emission current of 10 μA and Transmission Electron Microscopy (TEM), H9000NAR at 300 kV with a point-to-point image resolution of less than 0.2 nm, respectively. TEM samples were prepared by ion-beam milling (Chen and Fu, 2006). The Brunauer-Emmett-Teller (BET) specific surface areas of natural rutile powders were measured via nitrogen adsorption, using an accelerated surface area and porometry (Micromeritics ASPA 2010).

Natural rutile powders were immersed in methylene blue (MB) guaranteed reagent grade, $C_{16}H_{18}ClN_3S$, (Beijing Chemical Reagent Company) as a 1.0×10^{-5} mol dm^{-3} aqueous solution to carry out the photocatalytic reaction. Decom-

position and photocatalytic activity was evaluated from the decomposition of MB. One g rutile was added to 40 cm^3 of the solution and then irradiated by ultraviolet rays with an intensity of 1.6 mW cm^{-2} whilst continuously stirring with a magnetic stirrer. The change of concentration of MB in solution was determined from the relative absorbance at a wavelength of 665 nm in UV-VIS spectrum by using a calibration curve by an UV-Visible spectrophotometer (HP8453, Agilent Technologies Co. Ltd., China). The photocatalytic performance of rutile powders was simultaneously compared to the response of a commercial anatase control (HG-01, Huijinya Materials Ltd., Shanghai, China).

Results and discussions

Chemical composition of natural rutile

The chemical composition of rutile is listed in Table 1.

The formula of the natural rutile studied can be described as $(Ti_{0.971}V_{0.022}Zn_{0.005}Fe_{0.004}Cu_{0.002}Al_{0.003}P_{0.003}Nb_{0.002}Si_{0.002}Na_{0.002}Co_{0.001}Ca_{0.001}Ni_{0.001})_{1.019}O_2$, which approximates to $Ti_{1.019}O_2$. No Cr is present, but some OH was detected by IR spectroscopic measurements (Liu et al., 2003). The presence of significant oxygen vacancies (Jung et al., 2001) or a surplus of Ti in this natural rutile is assumed.

Table 1. *The chemical composition of natural rutile from Shaanxi Province, China (values in wt.%)*

TiO_2	V_2O_5	ZnO	FeO*	CuO	Al_2O_3	P_2O_5	Nb_2O_5	SiO_2	Na_2O	CoO	CaO	NiO	Total
96.49	1.22	0.36	0.39	0.22	0.16	0.11	0.14	0.21	0.03	0.05	0.03	0.08	99.49

* The total iron content is assumed to be present in the divalent state

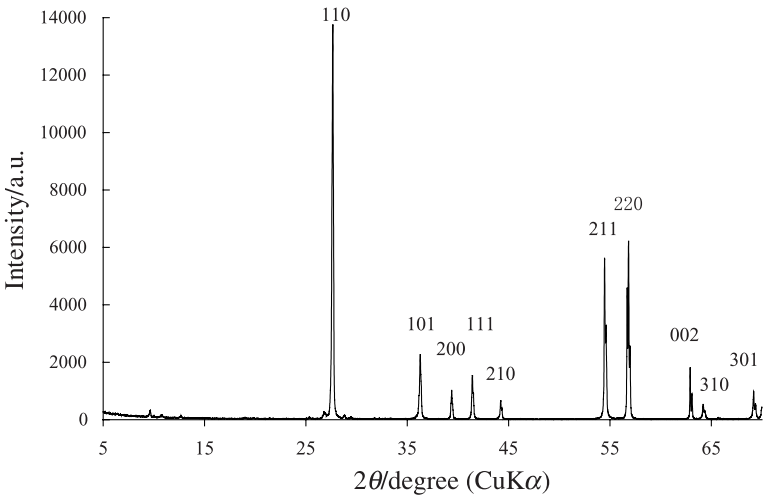

Fig. 1. XRD pattern of natural rutile from a rutile mine in a basalt in Shaanxi Province, China

X-ray diffraction of natural rutile

A representative XRD pattern of natural rutile is shown in Fig. 1. From a comparison of interlayer spacings d values and relative intensities (I/I_0) with the published data the sample was found to be pure rutile. The d values of the X-ray powder diffraction peaks assigned only to rutile. That complies with the ICDD entry for rutile, and JCPDS 21-1276 (Ohno et al., 2001). From its X-ray powder pattern natural rutile possesses the tetragonal unit cell parameters of $a_0 = 0.458$ nm, $c_0 = 0.295$ nm.

Morphology of natural rutile by FESEM

The morphology of natural rutile particles in different magnifications is shown in Fig. 2a, b. The size of the powders is in the range from ~100 to 300 μm. Natural rutile does not have smooth surfaces; rather there are a number of cracks and small protrusions, ~10 nm in size (Fig. 2c and d).

Micro-structure and morphology of natural rutile by HRTEM

The TEM image of natural rutile is shown in Fig. 3a and b, representing the (010) plane (Fig. 3c).

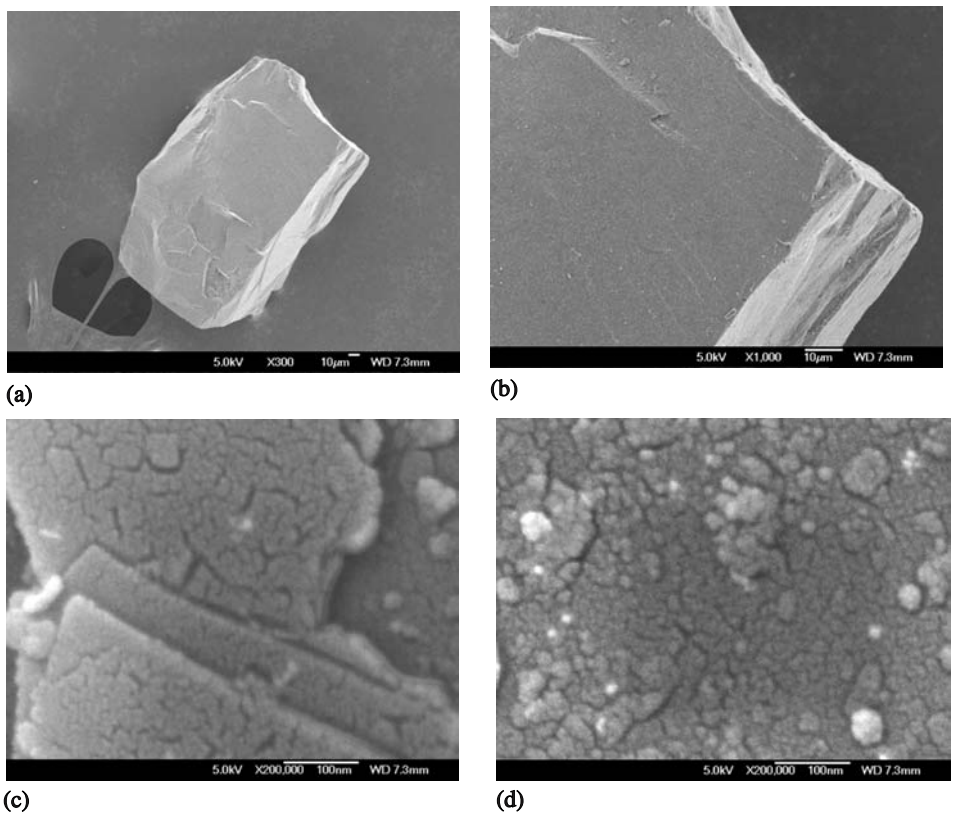

Fig. 2. FESEM images of natural rutile at different magnifications. (**a** and **b**) representative particles of rutile, (**c**) the representative surface of a rutile crystalline particle, (**d**) rutile surface showing cracks and small protrusions

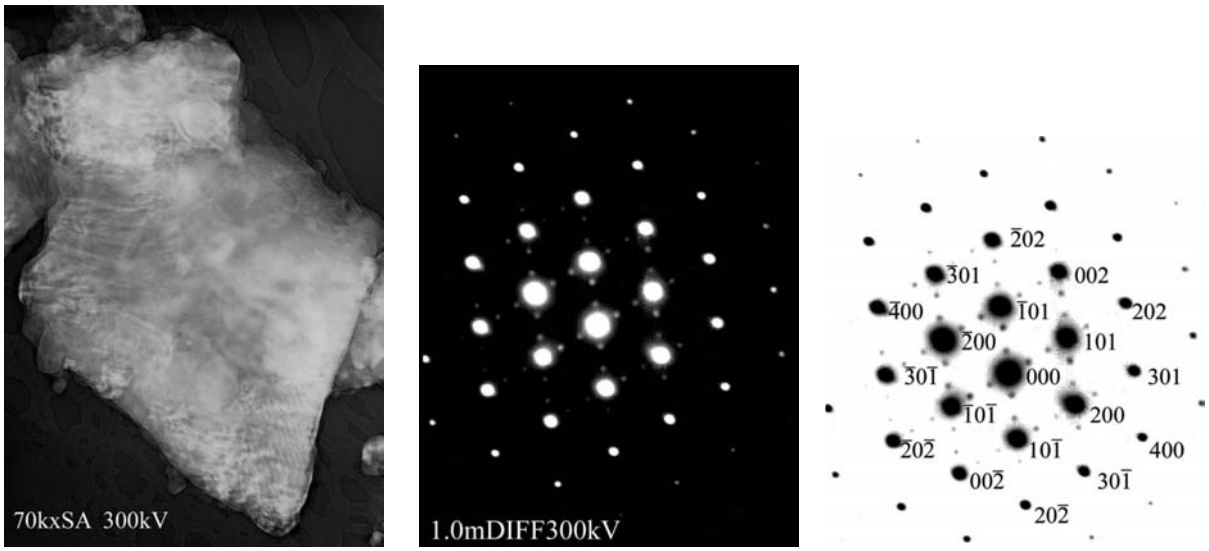

Fig. 3. (**a**) TEM image, (**b**) electron diffraction pattern and (**c**) indexing of the diffraction spots of natural rutile

As shown by the diffraction patterns in Fig. 3b, the satellite diffraction spots could often be observed along the [101] direction of different crystal zones in rutile, implying existence of (101) two-dimensional modulated structures (Meng et al., 2004; Wang et al., 2007). The satellite spots compose a centered rectangle around the matrix spots.

The high resolution TEM image of natural rutile is shown in Fig. 4. There are lattice fringes in two directions [101] and [$^{-}$, 101], in which $d_{101} = 0.247$ nm. Rutile displays some commensurate modulated structures along the [101] direction with repetition period of 0.736 nm (Fig. 4b), which is three times that of d_{101} for basic lattice fringes.

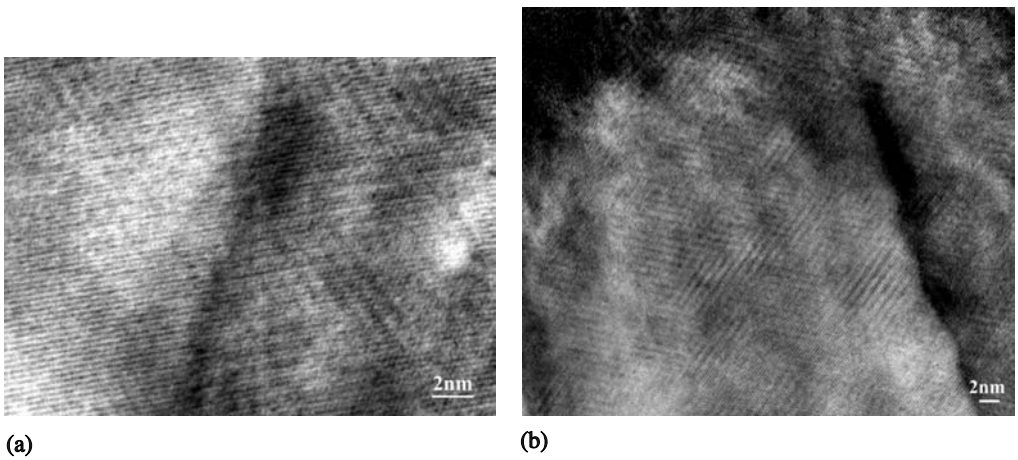

Fig. 4. (**a** and **b**) HRTEM images of rutile showing (101) lattice fringes ($d_{101} = 0.247$ nm)

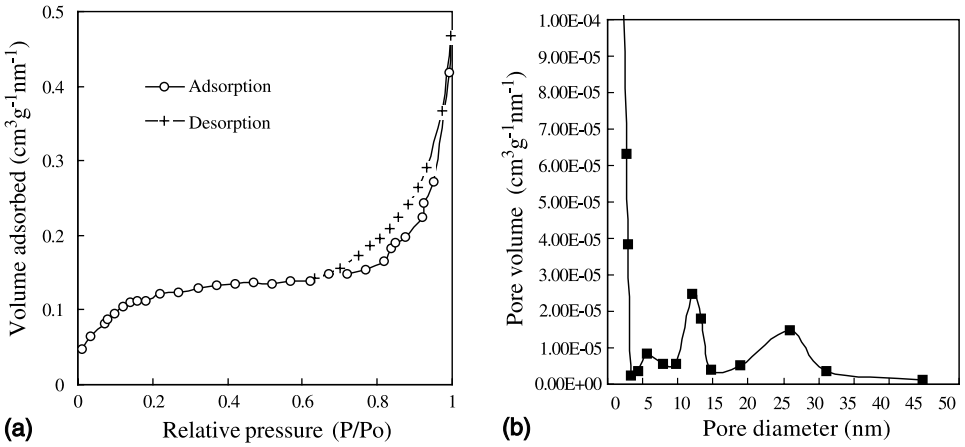

Fig. 5. (**a**) N_2 adsorption and desorption isotherms for natural rutile, (**b**) corresponding Barrett-Joyner-Halenda (BJH) pore size distribution of natural rutile powders determined from the N_2 adsorption branch isotherm

Adsorption of natural rutile

A N_2 adsorption-desorption isotherm is given in Fig. 5a. A hysteresis loop at high relative pressure is observed, which is related to the capillary condensation associated with large pore channels. It is similar to that of rutile nanoparticles synthesized by thermal hydrolysis of $TiOCl_2$ (Li et al., 2004).

The pore size distributions of natural rutile are shown in Fig. 5b. Barret-Joyner-Halenda (BJH) analyses show that natural rutile exhibits a mean pore diameter of 6.4 nm. Natural rutile has a wide ranged pore size distribution. However, Brunauer-Emmett-Teller (BET) specific surface area of natural rutile was only $0.4495\,m^2/g$.

Photocatalytic decomposition of methylene blue (MB)

Under UV irradiation, the decomposition of MB by natural rutile powders was evaluated by the change in the magnitude of MB absorbance and concentration

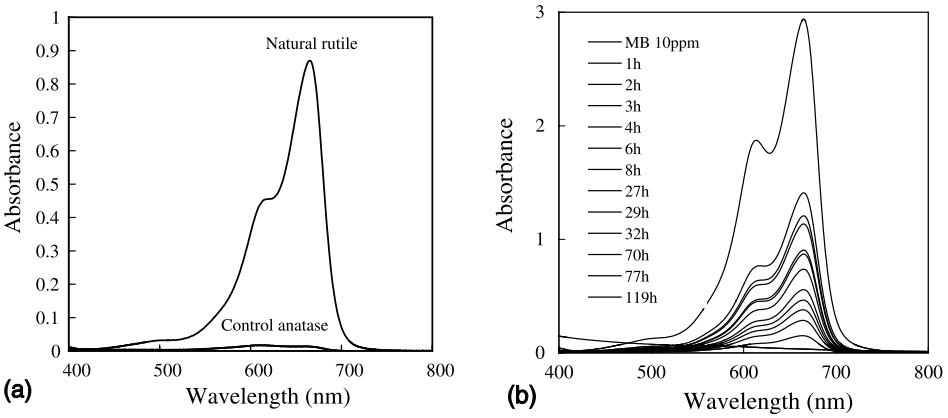

Fig. 6. Change of the absorbance curves of methylene blue solution with irradiation time of UV in the presence of natural rutile powders, (**a**) after 3 hours (**b**) from 0 to 119 hours (notice that the start is the top graph and intensity decreases with time)

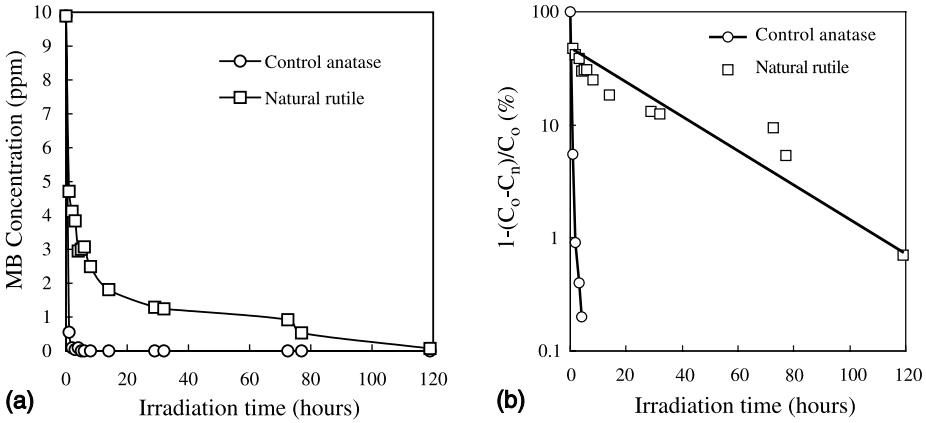

Fig. 7. (**a**) Changes in concentration of methylene blue with irradiation time and (**b**) plot of the value of $\{1 - \Delta C/C_0\} = \{1 - [(C_0 - C_n)/C_0]\}$ against irradiation time

with irradiation time. After three hours of UV irradiation, the MB was decomposed almost 100% by anatase and 50% by natural rutile (Figs. 6a and 7a). The decomposition by natural rutile is slower than that by the control anatase. However, ~90% MB was decomposed by natural rutile after 77 hours and after 119 hours practically no MB was detected (Figs. 6b and 7a). Although slower, natural rutile decomposed MB efficiently.

Changes in concentration of MB with irradiation time are shown in Fig. 7a. In order to evaluate the amount of MB decomposed, the concentration changes, $\Delta C/C_0 = (C_0 - C_n)/C_0$ (n = the photocatalytic reaction, hours) in different time were calculated for natural rutile and control anatase respectively, which was reasonably supposed to be the concentration decrease of MB due to photodecomposition. Therefore, in Fig. 7b the value of $\{1 - \Delta C/C_0\} = \{1 - [(C_0 - C_n)/C_0]\}$, which is the relative concentration of MB remaining in solution, was plotted in logarithmic scale against irradiation time. The relation can be approximated to be linear (Fig. 7b).

According to the linear relation, shown in Fig. 7b, which was assumed as reaction regression, a rate constant k of photocatalytic decomposition rate can be calculated. The rate reaction constants (k) derived from these linear relations, were $k = 1.787$ for anatase and $k = 0.359$ for natural rutile, respectively.

The rate reaction constant k of anatase is five times faster than that of rutile in the decomposition reaction. However, natural rutile maintained an acceptable ability of photocatalytic decomposition and decomposed most MB in one day and all of the MB in five days. However, the linear relationship is well developed for anatase, but there are some points which deviate from the regression line for rutile as evident in Fig. 7b. This implies a complex decomposition reaction process and mechanisms induced by complicated microstructures of natural rutile.

Rutile can be used as a promising photocatalyst for the decomposition of organic pollutants. It is possibly not efficient in fast flowing waters to decompose the organic contamination because of its lower decomposition rate, but it might be useful for remediation of contamination in quiet, still waters (e.g. pools, lakes) on a large scale.

Mechanism of photocatalytic property of natural rutile

Due to the small surface area, adsorption for MB by natural rutile is small. Thus, decomposition of MB is mainly induced by photocatalytic activity of rutile. The photocatalytic properties of rutile are believed to be related to ionic metal substitution (V^{5+}, Nb^{5+} and other metal impurities) and non-stoichiometry (Jung et al., 2001). About 3.5% Ti atoms in its crystalline structure substituted by V and Nb might induce the superstructures (Meng et al., 2004) and defects in rutile crystales (Figs. 2–4). Some of the metal impurities (V, Nb, Zn, Fe, Cu) might increase the photocatalytic activity of rutile, similar to what is known for anatase with V and with Sb and V (Choi et al., 1994; Stelzer et al., 2005; Bellifa et al., 2006). The irregular defect and impurities concentrations might be responsible for the disorientation of the linear relation in Fig. 7b. However, more work is still needed to test this hypothesis. Research on microstructures and properties would be helpful to explain this phenomenon.

Conclusions

Natural rutile was found to have good photocatalytic activity for methylene blue (MB). It decomposed 50% of MB in 3 hours, 90% in 77 hours and completely in 119 hours under UV irradiation. BET specific surface area of natural rutile was only $0.4495\,m^2/g$. Based on chemical composition and characterization of microstructure by XRD, FESEM and TEM, we propose that the good decomposition and photocatalytic properties of rutile result from ionic substitution and structural defects. Although the reaction constant of MB decomposition is only one fifth of anatase, natural rutile could be an effective alternative to anatase or other Ti-compounds for photocatalytic decomposition of organic pollutants.

Acknowledgements

The present work was supported by National Basic Research Program of China, 973 Program (No. 2007CB815602), National Natural Science Foundation of China (No. 50272005) and Analysis Foundation of Peking University in China. The authors would like to thank Prof. Li-Ping You for constructive discussions on TEM and Dr. Adrian Finch and Prof. Anton Beran for constructive suggestions and editorial handling.

References

Bellifa A, Lahcene D, Tchenar YN, Choukchou-Braham A, Bachir R, Bedrane S, Kappenstein C (2006) Preparation and characterization of 20 wt.% V_2O_5-TiO_2 catalyst oxidation of cyclohexane. Appl Catal A 305: 1–6

Chachula F, Liu Q (2003) Upgrading a rutile concentrate produced from Athabasca oil sands tailings. Fuel 82: 929–942

Chen J, Fu Z (2006) A-PbO_2-type nanophase of TiO_2 from coesite-bearing eclogite in the Dabie Mountains, China – comment. Am Mineral 91: 1699–1670

Choi W, Termin A, Hoffman MR (1994) The role of metal ion dopants in quantum-sized TiO_2: correlation between photoreactivity and charge carrier recombination dynamics. J Phys Chem l98: 13669–13679

Chuan X-Y, Hirano M, Inagaki M (2004) Photocatalytic performance and characterization of anatase-mounting natural porous silicate pumice. Appl Catal B 51: 255–260

Cristallo G, Roncari E, Rinaldo A (2001) Study of anatase-rutile transition phase in monolithic catalytic V_2O_5/TiO_2 and V_2O_5-WO_3/TiO_2. J Solid Chem 209: 249–256

Depero LE (1993) Coordination geometry and catalytic activity of vanadium on TiO_2 surface. J Solid State Chem 103: 528–532

Depero LE, Bonzi P, Musci M, Casale C (1994) Microstructural study of vanadium-titanium oxide powders obtained by laser-induced synthesis. J Solid State Chem 111: 247–252

El Goresy A, Chen M, Dubrovinsky L, Gillet P, Graup G (2001) An ultradense polymorph of rutile with seven-coordinated titanium from the Ries Crater. Science 293: 1467–1470

Gao Y, Chambers SA (1996) MBE growth and characterization of epitaxial TiO_2 and Nb-doped TiO_2 films. Mater Lett 26: 217–221

Inagaki M, Nakazawa Y, Hirano M, Kobayashi Y, Toyoda M (2001) Preparation of stable anatase-type TiO_2 and its photocatatlytic performance. J Inorg Mater 7: 809–811

Jaffe HW (1988) Crystal chemistry and refractivity. Cambridge University Press, Cambridge, pp 276–285

Jimmy CYL, Rayund WMK (1997) Enhanced photocatalytic activity of $Ti_{1-x}V_xO_2$ solid solution on the degradation of acetone. J Photochem Photobiol A Chem 111: 199–203

Jung D, Koo HJ, Dai D, Whangbo MH (2001) Electronic structure study of scanning tunneling microscopy image of the rutile TiO_2 (110) surface and their implications on the surface relaxation. Surf Sci 473: 193–202

Li N, Lu A, Qin S, Wang H, Li Q, Liu J (2003) Mineralogical characteristics of natural vanadiferous rutile gestating photocatalytic activity. Acta Petrol Mineral 22: 332–338 (in Chinese)

Li YZ, Lee NH, Lee EG, Song JS, Kim SJ (2004) The characterization and photocatalytic properties of mesoporous rutile TiO_2 powder synthesized through self-assembly of nano crystals. Chem Phys Lett 389: 124–128

Lin JY, Jimmy C, Lo D, Lam SK (1999) Photocatalytic activity of rutile $Ti_{1-x}Sn_xO_2$ solid solutions. J Catal 183: 368–372

Liu J, Lu A, Guo Y, Li N, Li Q (2003) Mineralogical characteristics of natural vanadiferous rutile gestating photocatalytic activity. Acta Petrol Mineral 22: 339–344 (in Chinese)

Meng DW, Wu XL, Meng X, Han YJ, Li DX (2004) Domain structures in rutile in ultrahigh-pressure metamorphic rocks from Dabie Mountains, China. Micron 35: 441–445

Ohno T, Sarukawa K, Tokieda K, Matsumura M (2001) Morphology of a TiO_2 photocatalyst (Degussa, P-25) consisting of anatase and rutile crystalline phases. J Catal 203: 82–86

Ollis DF, Al-Ekabi H (1993) Photocatalytic purification and treatment of water and air. Elsevier, Amsterdam, 89 p

Penn RL, Banfield JF (1998) Oriented attachment and growth, twinning, polytypism, and formation of metastable phases: insights from nanocrystalline TiO_2. Am Mineral 83: 1077–1082

Penn RL, Banfield JF (1999) Formation of rutile nuclei at $\{112\}$ twin interfaces and the phase transformation mechanism in nanocrystalline titania. Am Mineral 84: 871–876

Sánchez E, López T, Gómez R, Bokhimi MA, Novaro O (1996) Synthesis and characterization of sol-gel Pt/TiO_2 catalyst. J Solid State Chem 122: 309–314

Stelzer JB, Caro J, Fait M (2005) Oxidative dehydrogenation of propane on TiO_2 supported antimony oxide/vanadia catalysts. Catal Commun 6: 1–2

Sun J, Gao L, Zhang QH (2003) Synthesizing and comparing the photocatalytic properties of high surface area rutile and anatase titania nanoparticles. J Am Ceram Soc 86: 1677–1682

Towle SN, Brown GE, Parks GA (1999) Sorption of Co(II) on metal oxide surfaces: I. Identification of specific binding sites of Co(II) on (110) and (001) surfaces of TiO_2 (rutile) by grazing-incidence XAFS spectroscopy. J Colloid Interface Sci 217: 299–311

Tryba B, Morawski AW, Inagaki M (2003) Application of TiO_2-mounted activated carbon to removal of phenol from water. Appl Catal B 41: 427–433

Tsuji H, Sagimori T, Kurita K, Gotoh Y, Ishikawa J (2002) Surface modification of TiO_2 (rutile) by metal negative ion implantation for improving catalytic properties. Surface Coatings Technol 158/159: 208–213

Wang YM, Warschkow O, Marks LD (2007) Surface evolution of rutile TiO_2 (100) in an oxidizing environment. Surface Sci 601: 63–67

Zack T, Luvizotto GL (2006) Application of rutile thermometry to eclogites. Mineral Petrol 88: 69–85